Nanotechnology

PAPER

Modeling pyramidal silicon nanopores with effective ion transport

To cite this article: Feibin Xiang *et al* 2022 *Nanotechnology* **33** 485503

View the article online for updates and enhancements.

You may also like

- A generalized energy transfer model for squeeze-film air damping in the free molecular regime
Cunhao Lu, Pu Li, Minhang Bao et al.
- Derivation of Effective Chiral Lagrangian Involving PSGB and Vector Bosons from QCD
Wang XueLei and Wang Qing
- Reducing scattered light in LIGO's third observing run
S Soni, C Austin, A Effler et al.

IOP ebooks™

Bringing together innovative digital publishing with leading authors from the global scientific community.

Start exploring the collection–download the first chapter of every title for free.

This content was downloaded from IP address 130.203.198.60 on 12/09/2022 at 17:04

IOP Publishing Nanotechnology
Nanotechnology 33 (2022) 485503 (10pp) https://doi.org/10.1088/1361-6528/ac8c9c

Modeling pyramidal silicon nanopores with effective ion transport

Feibin Xiang[1,2], **Ming Dong**[3], **Wenchang Zhang**[1], **Shengfa Liang**[1] and **Weihua Guan**[3,4,*]

[1] Key Laboratory of Microelectronics Devices & Integrated Technology, Institute of Microelectronics, Chinese Academy of Sciences, Beijing 100029, People's Republic of China
[2] University of Chinese Academy of Sciences, Beijing 100049, People's Republic of China
[3] School of Electrical Engineering and Computer Science, Pennsylvania State University, University Park, PA, 16802, United States of America
[4] Department of Biomedical Engineering, Pennsylvania State University, University Park, PA, 16802, United States of America

E-mail: wzg111@psu.edu

Received 7 April 2022, revised 17 August 2022
Accepted for publication 25 August 2022
Published 12 September 2022

Abstract

While the electrical models of the membrane-based solid-state nanopores have been well established, silicon-based pyramidal nanopores cannot apply these models due to two distinctive features. One is its 35.3° half cone angle, which brings additional resistance to the moving ions inside the nanopore. The other is its rectangular entrance, which makes calculating the access conductance challenging. Here, we proposed and validated an effective transport model (ETM) for silicon-based pyramidal nanopores by introducing effective conductivity. The impact of half cone angle can be described equivalently using a reduced diffusion coefficient (effective diffusion coefficient). Because the decrease of diffusion coefficient results in a smaller conductivity, effective conductivity is used for the calculation of bulk conductance in ETM. In the classical model, intrinsic conductivity is used. We used the top-down fabrication method for generating the pyramidal silicon nanopores to test the proposed model. Compared with the large error (⩾25% in most cases) when using the classical model, the error of ETM in predicting conductance is less than 15%. We also found that the ETM is applicable when the ratio of excess ion concentration and bulk ion concentration is smaller than 0.2. At last, it is proved that ETM can estimate the tip size of pyramidal silicon nanopore. We believe the ETM would provide an improved method for evaluating the pyramidal silicon nanopores.

Supplementary material for this article is available online

Keywords: pyramidal silicon nanopore, cone angle, effective diffusion coefficient, effective conductivity, concentration limit, size estimation

(Some figures may appear in colour only in the online journal)

1. Introduction

Attributed to high throughput, label-free and adjustable size, solid-state nanopore sensors have become a type of novel analysis tool for ions [1, 2], DNA [3–5], protein [6–9], and nanoparticles [10, 11]. At present, the widely used methods of nanopore fabrication include focused electron/ion beam [7, 12], laser-assisted pulling [6, 13], tracked etching [14, 15] and controlled breakdown [16, 17]. However, these methods have the main disadvantages of low efficiency or poor size uniformity. Compared with nanopores fabricated in these ways, pyramidal silicon nanopore [8, 18–20] is based on the traditional semiconductor processes. Therefore, pyramidal silicon nanopore has the potential for large-scale and batch production. Based on the coulter principle, when a molecule passes through a pyramidal silicon nanopore, the current will drop to generate a pulse. The

* Author to whom any correspondence should be addressed.

 © 2022 IOP Publishing Ltd

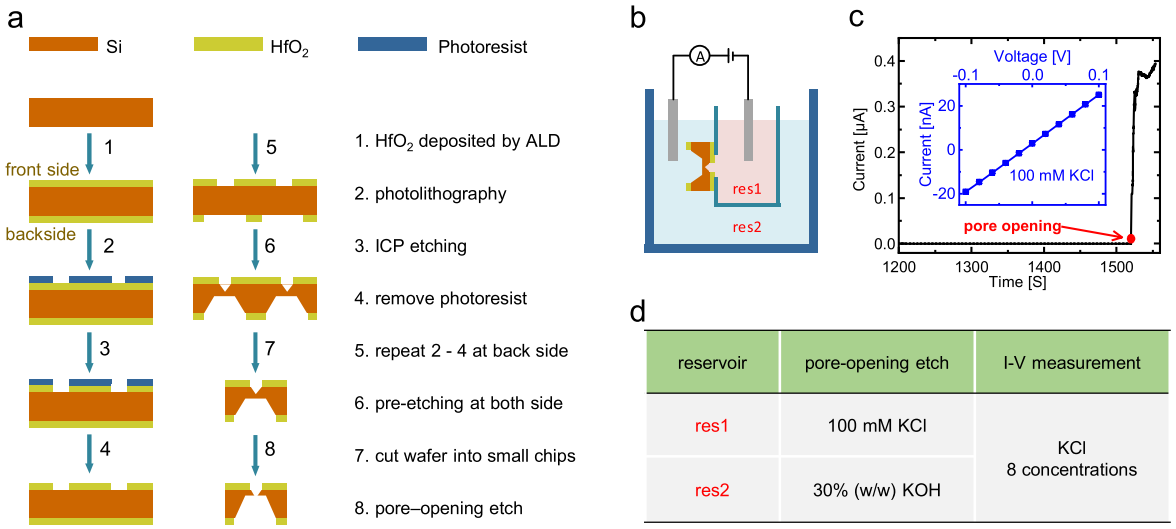

reservoir	pore-opening etch	I-V measurement
res1	100 mM KCl	KCl 8 concentrations
res2	30% (w/w) KOH	

Figure 1. The fabrication and electrical measurement of the pyramidal silicon nanopores. (a) The fabrication process of a pyramidal silicon nanopore. In step 6, the wafer is immersed into the KOH solution for pre-etching on both sides. (b) The system for the pore-opening etch and the current–voltage (*I–V*) measurement. 'res1' and 'res2' represent two reservoirs in the system. The electrodes are Pt in the pore-opening etching and Ag/AgCl in the *I–V* measurement. (c) The current trace when nanopore opening. Inset: *I–V* curve of a pyramidal silicon nanopore (100 mM KCl). (d) The solutions in two reservoirs of (b) are dependent on the applications. KCl solution with 8 different concentrations (100 mM and 16 mM to 1000 mM with gradient) is used for *I–V* measurement.

shape of the pulse can reflect the information of the target molecule [8, 10, 11]. Hence, knowledge of its electrochemical properties is required for the applications of pyramidal silicon nanopores. The transport of ions in a nanopore system is influenced by bulk, entrance and surface. The three parts correspond to bulk conductance, access conductance (i.e. access resistance) and surface conductance [21]. And the series and parallel connections of three conductance constitute the total nanopore conductance [22].

In fact, to obtain a better signal-to-noise ratio [23–25], most molecular analysis experiments such as DNA diagnosis [3, 5] and characterization of protein [7, 26], are performed under high electrolyte concentration. At this time, the surface conductance can be neglected [27]. Based on this premise, many classical models only considering bulk and access have been proposed to describe the electrical behavior of kinds of nanopores [16, 21, 28, 29]. In these models, intrinsic conductivity is used for the calculation of bulk conductance. Taking into account the shape of the nanopore entrances, equipotential disks are applied for calculating access conductance [21]. However, these methods are not suitable for pyramidal silicon nanopores. First, when particles pass through a non-columnar channel, the diffusion coefficient decreases. The magnitude of the decrease is related to the half cone angle of the channel [30]. The reduction in the diffusion coefficient will result in a smaller conductivity, according to the definition of conductivity [21]. The half cone angle of pyramidal silicon nanopore is 35.3° [8]. Thus, it is necessary to consider the influence of smaller conductivity on bulk conductance. Secondly, the shape of the entrance of the pyramidal silicon nanopore is rectangular or square [8, 20], which means that the calculation of the access also needs to be modified. Previously, Wen *et al* [31, 32] proposed an analytical model based on the distribution of electrical fields, but it is only applicable to that pyramidal silicon nanopore with a square entrance. Therefore, from the point of view of ion transport, a more comprehensive model is necessary for the pyramidal silicon nanopore.

In this work, we establish a new electrical model—effective transport model (ETM). The model can describe the electrical behavior of the pyramidal silicon nanopore with rectangular entrances. After considering the impact of 35.3° half cone angle, an effective diffusion coefficient [30] is used inside the pyramidal silicon nanopore. Correspondingly, the conductivity is also scaled based on the relationship between intrinsic diffusion coefficient and effective diffusion coefficient. On the other hand, two rectangular disks are used to calculate the access conductance at both entrances. The model is validated by experiments. The impact of the effective diffusion coefficient and the access effect is demonstrated by the comparison between comparing three different models—bulk conductance model (BCM), classical model and ETM. Besides, the concentration limit of ETM is discussed. At last, it is proved that the model can be used for the estimation of the tip size of the pyramidal silicon nanopore.

2. Experimental section

2.1. Nanopore fabrication

Pyramidal silicon nanopores are fabricated in a 200 μm thick N-type <100> silicon wafer (Rdmicro Corp, Suzhou, China). The process of nanopore fabrication is shown in figure 1(a). In step 1, 50 nm thick hafnium oxide (HfO_2) is grown on both sides of the wafer through atomic layer deposition. An array (10 or 20 μm square, 5 $\times$ 5) is transferred to the front side of the silicon wafer by photolithography (step 2) and ICP etching (step 3). The HfO_2 in windows is etched in step 3 and the residual photoresist is removed in step 4. Another array

with larger windows (320 μm square, 5 $\times$ 5) is transferred to the backside of the silicon wafer through step 5. The arrays on the front side and back side are aligned by lithography. Next, the exposed silicon of both sides is etched with 30% (w/w) potassium hydroxide (KOH) at 70 °C (pre-etching in step 6). The etching depth can be inferred through the size of inverted pyramids on both sides. When the thickness of the remaining silicon is about 10 μm, the etching process is stopped and the wafer is cut into small chips (step 7). In the pore-opening etch (step 8), a small chip is fixed on a polytetrafluoroethylene (PTFE) reservoir by Polydimethylsiloxane (PDMS) and Apiezon W. The system for pore-opening etch is shown in figure 1(b). The solutions in reservoirs are introduced in figure 1(d). The backside is etched by 30% (w/w) KOH (40 °C). The front side includes an inverted pyramid with a sharp tip, and the side contacts with 100 mM potassium chloride (KCl) solution. The leakage current is monitored by Keithley 2636B (Tektronix, USA) and a pair of platinum (Pt) electrodes. The current will increase rapidly when the pore forms, as shown in figure 1(c). At this time, the etching process is stopped in deionized water.

2.2. Nanopore characterization with scanning electron microscope (SEM) and I–V

The characterization of pyramidal silicon nanopore is performed by SEM imaging and electrical (*I–V*) measurement. For SEM imaging, the images are acquired using SUPRA 55 SAPPHIRE (Carl Zeiss, Germany). The SEM image of the front side (bottom side) of a pyramidal silicon nanopore is shown in figure 2(b). And figure 2(c) presents the image of the backside (tip side).

In the *I–V* measurement, the pyramidal silicon nanopore is fixed on the PTFE reservoir by PDMS (figure 1(b)), similar to the system for pore-opening etch. As introduced in figure 1(d), the *I–V* measurements are performed in 8 different concentrations of KCl solution (100 mM and 16 mM to 1000 mM with gradient), respectively. The KCl solutions from 16 to 500 mM are obtained from gradient dilution of 1000 mM KCl solution. From −0.1 to 0.1 V bias (step: 0.02 V), the bias voltage is applied by Keithley 2636B. A pair of silver/silver chloride (Ag/AgCl) electrodes is used to monitor the current. A typical *I–V* curve of a pyramidal silicon nanopore is shown in the inset of figure 1(c).

3. Physical model

Pore conductance is related to its geometry [27, 28, 33]. The schematic diagram of a typical pyramidal silicon nanopore is demonstrated in figure 2(a). h represents the thickness of the supporting layer, in other words, the length of the nanopore in the axial direction (z-axis). Attributed to the manufacturing errors of the masks and defects of the wafer, the shape of the pore tip is usually a rectangle instead of a standard square [20], and the phenomenon is confirmed by SEM images (figures 2(b) and (c)). Two adjacent sides of the pore tip are donated by a and b, which can be measured by SEM. Here, we call the longer side a. And two adjacent sides of the pore bottom are represented by L_a and L_b. Because the bottom window size is very large in this work, the impact of manufacturing errors on window size can be neglected. So L_a is almost equal to L_b. The sloped angle (β) is 54.7° resulting from the orientation selectivity of KOH wet etching. Thus, the half of the cone angle (α) is 35.3°.

The conductance of a nanopore is contributed by three parts: (a) bulk: ions of the bulk solution inside the nanopore [21]; (b) access: the convergence effect of electric field lines from the reservoir to the entrances of the nanopore [34, 35]; (c) surface: excess ions neutralizing the fixed charges located in the pore sidewalls [36]. Here, we only consider the pyramidal silicon nanopore conductance under high electrolyte concentration. In this situation, the excess ion concentration is much smaller than the bulk ion concentration. Therefore, the surface conductance is neglected. And the total conductance (G_t) is equal to the series connection of the bulk conductance (G_b) and the access conductance (G_a). The ions are considered to be in equilibrium, i.e. the ion concentration is uniform in the whole system. In the classical model for calculating nanopore conductance, the conductivity of the system is considered to be equal to the intrinsic conductivity of the electrolyte solution [21].

However, according to Zwanzig's work [30], when passing through a non-columnar channel, particles (e.g. ions) need extra time to find their way out of the cross-section. This effect will lead to a reduction in the diffusion coefficient (D_i). The smaller diffusion coefficient can be expressed as effective diffusion coefficient ($D_{i,eff}$). In this work, i (= K^+, Cl^-) represents the type of ion. In the channel, the effective diffusion coefficient ($D_{i,eff}$) [30, 37] is

$$D_{i,eff}(z) \approx \frac{D_{i,ins}}{1 + \gamma[L'_z(z)]^2}, \tag{1}$$

where $D_{i,ins}$ is the intrinsic diffusion coefficient of ith ion. γ is a parameter related to the geometry of the channel. In detail, γ is 1/12 for a two-dimensional channel and 1/8 for a conical (three-dimensional) channel [30, 38]. As shown in figure 3(a), $L_z(z)$ is the z-dependent channel width

$$L_z(z) = L_0 + z \cdot 2\tan\alpha, \tag{2}$$

L_0 is the width of the tip. The conductivity (σ) is [21]

$$\sigma = \frac{z_i^2 F^2}{RT}\sum_i D_i c_i, \tag{3}$$

z_i (=1 for K^+, −1 for Cl^-) is the valence of the ith ion. F (96 485 C mol^{-1}) is Faraday constant. R is the universal gas constant. T is the temperature. c_i is the concentration of the ith ion. From equation (3), the decreasing diffusion coefficient will lead to a smaller conductivity.

The conical nanopore widely used, e.g. PET nanopore [39, 40] and glass nanopipette [29], has a small α (close to 0°). $D_{i,eff}$ inside channel is approximate to $D_{i,ins}$. Thus, the classical model applies to these nanopores. Besides, these nanopores usually have another feature: a large aspect ratio. At this time, G_a is much smaller than G_b, so the classical model can be simplified into the BCM in which the

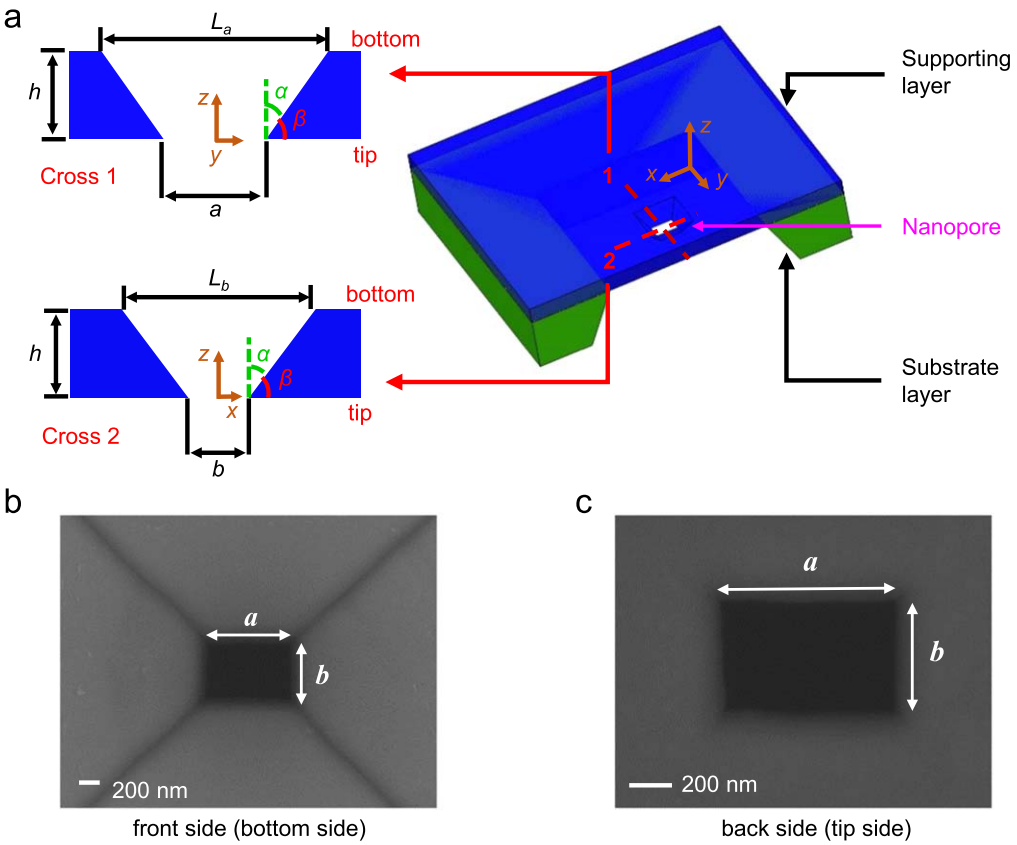

Figure 2. (a) The schematic diagram of the structure of a top-down fabricated pyramidal silicon nanopore (not in scale). The masking layer (HfO_2) is not shown. It is worth noting that the supporting layer and the substrate layer belong to the same wafer. And two colors are only used to highlight the nanopore and do not represent two different divided materials. The SEM images of a typical pyramidal silicon nanopore are pictured from (b) the front side (bottom side) and (c) the backside (tip side). '*a*' and '*b*' represent the long edge and short edge of the nanopore tip.

total nanopore conductance is approximately equal to bulk conductance.

However, these geometry limits are not met in pyramidal silicon nanopores. First, α is 35.3°, and so $L_z'(= 2\tan\alpha)$ is $\sqrt{2}$, which means the deviation of diffusion coefficient cannot be neglected. Therefore, it is necessary to re-calculate conductivity inside pyramidal silicon nanopores. On the other hand, although h (10–20 μm) is much larger than tip size (a and b, <1 μm), bottom size (L_a and L_b) may exceed h ($L_a = a + 2h{\cdot}\tan\alpha$). So the contribution of G_a on G_t should be evaluated. In order to figure out these questions, three different physical models are established.

3.1. Classical model

The equivalent circuit diagram of the classical model is shown in figure 3(b). In this model, the conductivity in the whole system is intrinsic (σ_{ins}). In other words, we do not consider the impact of decreasing diffusion coefficient. The bulk conductance is represented by $G_{b,ins}$

$$G_{b,ins} = \sigma_{ins}\left(\int \frac{dz}{s(z)}\right)^{-1}. \tag{4}$$

According to equation (2), $s(z)$ $(= [\sqrt{2}z + a][\sqrt{2}z + b])$ is the z-dependent area of the cross-section distanced from the pore tip along the nanopore axis (z-axis). It is emphasized that the mathematical expression is different when $a = b$ and $a \neq b$. Considering the factors above, the result is

$$G_{b,ins} = \sigma_{ins} \cdot \begin{cases} \sqrt{2} \cdot diff \cdot \left(\ln\left(\dfrac{\sqrt{2}h + b}{\sqrt{2}h + a}\right) + \ln\left(\dfrac{a}{b}\right)\right)^{-1}, a \neq b \\ \sqrt{2}\left(-\dfrac{1}{\sqrt{2}h + a} + \dfrac{1}{a}\right)^{-1}, a = b \end{cases}, \tag{5}$$

where *diff* $(= a - b)$ is the difference between two adjacent edges of the pore tip.

The access conductance consists of $G_{a,t}$ and $G_{a,b}$, which are the access conductance at the pore tip and the bottom, respectively. Based on the Hall model [21, 41], $G_{a,t}$ and $G_{a,b}$ are calculated by

$$G_{a,t} = \sigma_b \cdot C_t/(2\varepsilon_r\varepsilon_0) \tag{6}$$

$$G_{a,b} = \sigma_b \cdot C_b/(2\varepsilon_r\varepsilon_0), \tag{7}$$

where ε_r $(= 78.5)$ and ε_0 $(= 8.85 \times 10^{-12}$ F m$^{-1})$ are the relative permittivity of electrolyte solution and the vacuum dielectric constant, respectively. C_t and C_b are the capacitances of

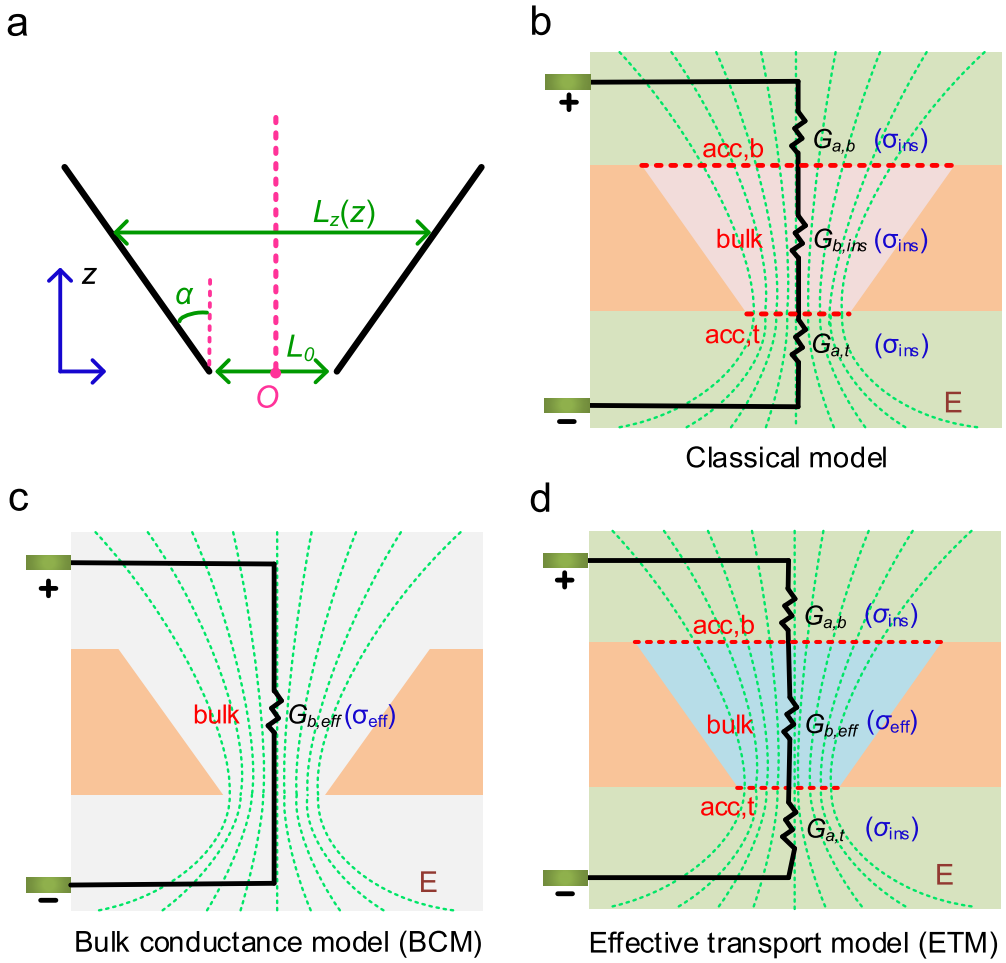

Figure 3. (a) The schematic diagram of a typical non-columnar channel. L_O is the length of the tip of the channel. O is the origin. (b) The classical model. (c) The bulk conductance model (BCM). (d) The effective transport model (ETM). The red dashed lines in (b) and (d) represent the two entrances. In these models, 'bulk', 'acc,b' and 'acc,t' represent three different effects: the drift of bulk ions inside the nanopore, access effect at the bottom and access effect at the tip. 'E' represents the electrical field and green lines represent electrical field lines. 'σ_{eff}' and 'σ_{ins}' represent effective conductivity and intrinsic conductivity, respectively.

the equipotential disks representing the tip and the bottom, respectively. Because of the rectangular shape, the two capacitances are [35]

$$C_t = 2\pi\varepsilon_r\varepsilon_0 a/\ln(4a/b) \tag{8}$$

$$C_b = 2\pi\varepsilon_r\varepsilon_0 L_a/\ln(4L_a/L_b). \tag{9}$$

As the result, G_t is

$$G_t = (G_{b,ins}^{-1} + G_{a,t}^{-1} + G_{a,b}^{-1})^{-1}. \tag{10}$$

The length of the pyramidal silicon nanopore can be acquired by $h = (L_a - a)/(2\tan\alpha)$ based on equation (2). In this work, L_a (>10 μm) is much larger than a (<1 μm). So, h can be roughly estimated by $L_a/(2\cdot\tan\alpha)$.

3.2. Bulk conductance model

The equivalent circuit diagram of the classical model is shown in figure 3(c). In this model, G_t is considered equal to the bulk conductance. However, different from the classical model, the decrease in the diffusion coefficient is taken into account. However, the previous research on $D_{i,eff}$ mainly focused on 2D channels or 3D channels with circular cross-sections [30, 38, 42–44]. As far as we know, there is no study of $D_{i,eff}$ in the pyramidal structure. The reason may be that the non-circular section makes the calculation difficult. Therefore, for simplicity, we apply $D_{i,eff}$ of the conical channel in the pyramidal silicon nanopore. Because compared with the two-dimensional channel, pyramidal silicon nanopore is closer to the three-dimensional conical channel. In conical structure, γ is 1/8. Because α is 35.3°, $D_{i,eff}$ is equal to $0.8D_{i,ins}$ according to equation (1). Assuming the concentration is uniform in the system, the effective conductivity (σ_{eff}) inside the pyramidal silicon nanopore is $0.8\sigma_{ins}$. Therefore, the effective bulk conductance ($G_{b,eff}$) is equal to $0.8G_{b,ins}$

$$G_{b,eff} = \sigma_{eff}\left(\int\frac{dz}{s(z)}\right)^{-1} = 0.8\sigma_{ins}\left(\int\frac{dz}{s(z)}\right)^{-1}. \tag{11}$$

3.3. Effective transport model

The equivalent circuit diagram of the classical model is shown in figure 3(d). Similar to the classical model, G_t is equal to the series connection of access conductance and bulk conductance. The

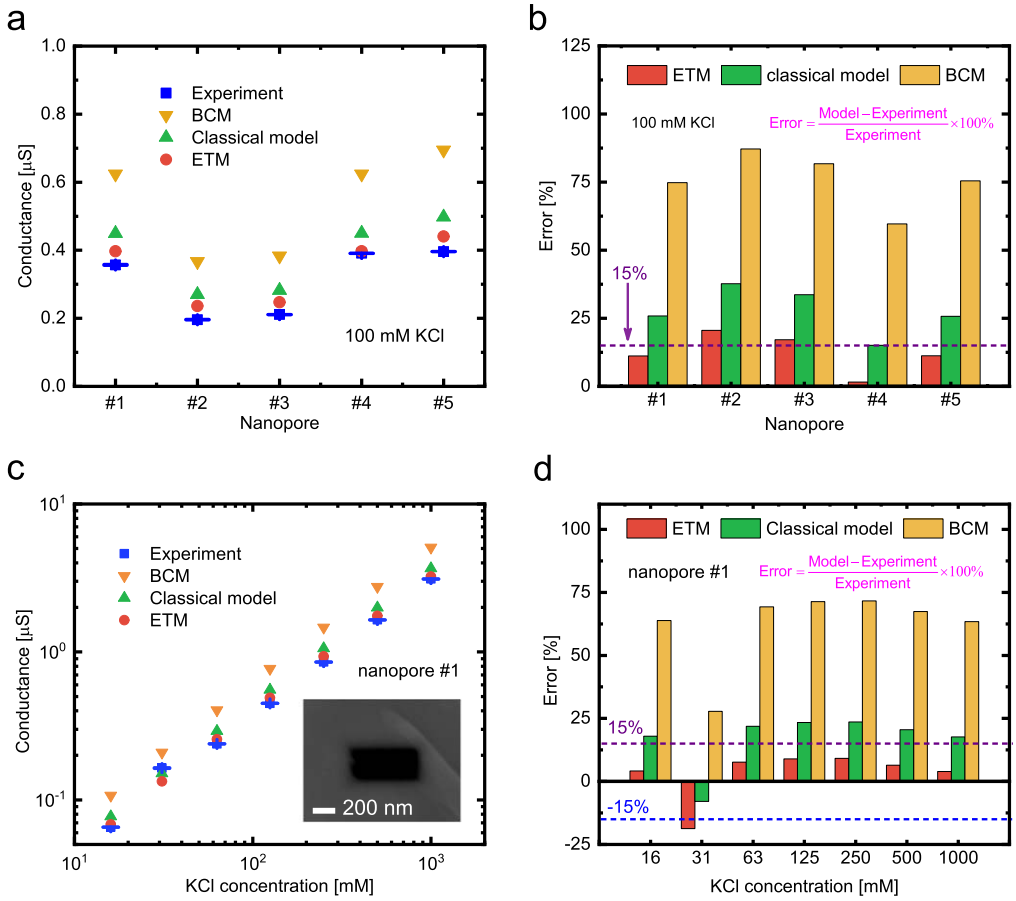

Figure 4. The validation of three models using the experiment results. (a) The comparison between theoretical values calculated from BCM, classical model and ETM and measured conductance for 5 different pyramidal silicon nanopores under 100 mM KCl concentration. The sizes of 5 nanopores are introduced in table 1. (b) The relative errors between three models and experiment in (a). (c) The comparison between three models and measured conductance under 7 different KCl concentrations (16–1000 mM with gradient) for nanopore 1. Inset: SEM image of nanopore 1 pictured from tip side. (d) The relative errors between three models and experiment from (c). The error bars shown in (a) and (c) represent a standard deviation from three consecutively measurements. The purple and blue dashed lines in (b) and (d) represent 15% and −15%, respectively.

difference is the decreasing diffusion coefficient is in consideration. Therefore, σ_{ins} is used in the calculation of $G_{a,t}$ and $G_{a,b}$, as shown in equations (6) and (7). σ_{eff} is used in the calculation of $G_{b,eff}$ as shown in equation (11). In this model, G_t is

$$G_t = (G_{b,eff}^{-1} + G_{a,t}^{-1} + G_{a,b}^{-1})^{-1}. \tag{12}$$

Table 1. The geometry of 5 nanopores for model validation.

Nanopore	a (nm)	b (nm)	h (μm)
#1	600	278	10
#2	375	158	20
#3	385	169	20
#4	758	200	10
#5	724	276	10

4. Results and discussion

In section 4.1, the ETM was validated using the experimental results of 5 pyramidal silicon nanopores. Since ETM only considers nanopores under high electrolyte concentration, the concentration limit is discussed in section 4.2. Finally, in section 4.3, ETM is used for the size prediction of pyramidal silicon nanopore tip.

4.1. Validation of ETM

The conductances of five different pyramidal silicon nanopores (nanopore #1–5) are used to validate the three models. The sizes of the 5 nanopores are shown in table 1. The conductances are measured in 100 mM KCl solution ($\sigma_b = 1.28$ S m^{-1} from table S1). The results are shown in figure 4(a) and the relative errors are shown in figure 4(b). It can be found that compared with experiments, the classical model has a relatively large deviation (⩾25% in most cases). The relative errors in nanopores #2 and #3 even exceed 30%. After considering the decrease of diffusion coefficient, ETM is closer to experiments. On the other hand, there is also a huge deviation between BCM and experiment.

To get a more comprehensive evaluation, based on nanopore #1, the three models are further tested under

different KCl concentrations ranging from 16 to 1000 mM. The predicted nanopore conductance and experimental values are shown in figure 4(c), and the relative errors are shown in figure 4(d). The conductivity of the KCl solution does not increase with concentrations linearly [21, 45], and their relationship is shown in figure S1 (available online at stacks.iop.org/NANO/33/485503/mmedia). The detailed values are shown in table S1. The comparisons and relative errors of nanopores #2–5 are shown in figure S2(a)–(h). Compared with the other two models, the conductance predicted by ETM is closer to experiments. Overall, the relative errors between ETM and measured conductance are within 15%. The results prove that: (1) in non-columnar channels with a large half cone angle, the reduction of diffusion coefficient should be taken into account; (2) the access effect has a great contribution to the conductance of pyramidal silicon nanopores.

Although ETM has a better performance compared with the classical model, the error still exists between the predicted value and the experimental result. It may be originated from the approximation of the diffusion coefficient. The change in channel geometry can affect the effective diffusion coefficient, according to the difference in $D_{i,eff}$ in 2D channel and 3D conical channel [30]. Similarly, it can be speculated that $D_{i,eff}$ is also different in the pyramidal structure and the conical channel. Therefore, $D_{i,eff}$ used is not the real effective diffusion coefficient of the pyramidal silicon nanopore.

4.2. Concentration limit

For a long time, it was believed that when the thickness of the Debye layer is much smaller than the nanopore radius, the effect of surface charge can be ignored [21]. However, recently, Poggioli *et al* [46] and Dal Cengio *et al* [47] proved that the criterion is the ratio between excess ion concentration and bulk ion concentration, which is characterized by Dukhin number (Du). At z-position dependent cross-section, excess ion concentration is

$$X(z) = -\frac{Q_s L_s(z)}{Fs(z)}, \tag{13}$$

where Q_s is the surface charge density and set to -0.016 C m^{-2} in pyramidal silicon nanopore [8]. So the excess ion is K^+. L_s $(= 4\sqrt{2}z + 2a + 2b)$ is perimeter of the z-position dependent cross-section.

According to Donnan equilibrium [48], the co-ion (i.e. Cl^-) concentration is

$$c_{Cl^-}(z) = -\frac{X(z)}{2} + \sqrt{\left(\frac{X(z)}{2}\right)^2 + c_{res}^2}, \tag{14}$$

c_{res} is the electrolyte concentration in the reservoir. The Dukhin number is

$$Du(z) = \frac{X(z)}{2c_{Cl^-}(z)}. \tag{15}$$

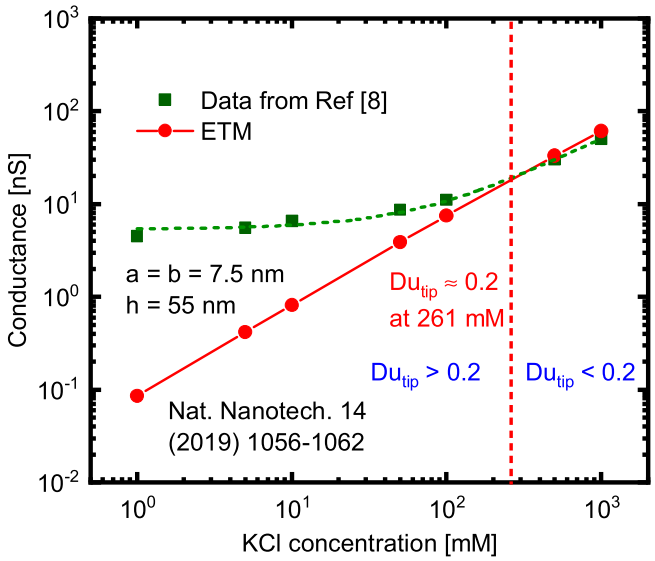

Figure 5. The concentration limit of ETM based on the pyramidal silicon nanopore from the [8]: $a = b = 7.5$ nm and $h = 55$ nm. Red solid line: predicted conductance as the function of KCl concentration based on ETM. Green dashed line: the fitted curve of measured conductance. Red dashed line: KCl concentration is 261 mM and Du_{tip} is 0.2 under the concentration.

Considering the pore tip is the region with the largest ion selectivity, we focus on the Du of tip (Du_{tip}), i.e. $z = 0$.

Figure 5 shows the conductance of a 7.5×7.5 nm pyramidal silicon nanopore at varied KCl concentrations from Zeng *et al* [8]. The values predicted by ETM at low concentrations (1–100 mM KCl) are much smaller than the experimental results. And the model is consistent with the experiment at high concentrations (500–1000 mM KCl). It can be found that the ion concentration (261 mM) satisfying $Du_{tip} = 0.2$ is between 100 and 500 mM. On basis of the result, it can be concluded that ETM can describe the electrical behavior of silicon pyramidal nanopore when Du_{tip} is smaller than 0.2. The conclusion can also explain why ETM is applicable in our pyramidal silicon nanopores under 16 mM. Taking nanopore #1 as an example, at 16 mM, Du_{tip} is 0.06, which is still smaller than the limit (0.2).

The failure of ETM at low concentrations is mainly due to the effect of surface charge. In ETM, surface conductance is neglected. However, under low concentrations, the ions in the nanopore are mainly excess ions [27, 36]. At this time, surface conductance dominates the conductance inside the nanopore. Therefore, ETM is not suitable for nanopores at low concentrations.

4.3. Size estimation

Estimating nanopore size through the measured conductance has been widely used, especially for the nanopores fabricated in a liquid environment [14, 16, 17], because of the negative effects from the electron microscope [49–51] and corresponding pre-treatment. The SEM images of a typical pyramidal silicon nanopore before and after pore-opening etch are shown in figures 6(a) and (b), respectively. Figure 6(a) shows L_{line} is the length of the line located at the tip of the inverted

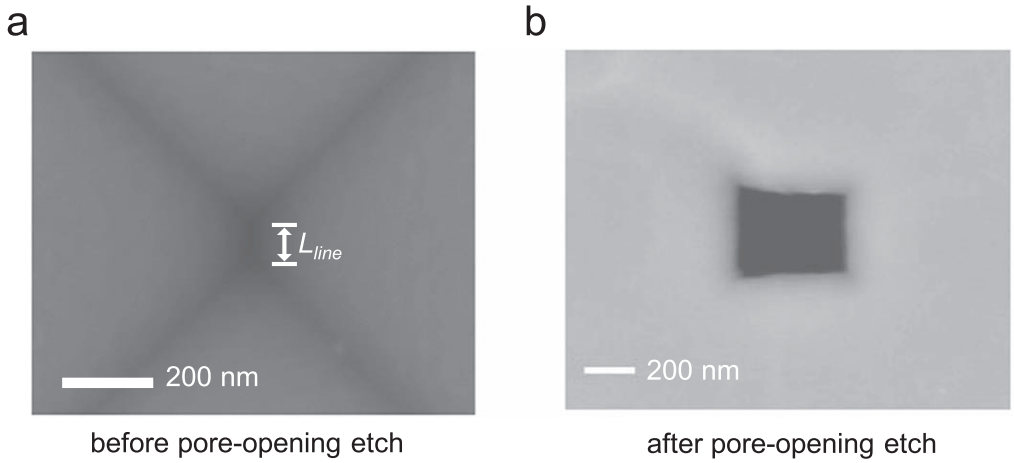

Figure 6. The SEM images of a typical pyramidal silicon nanopore (a) before and (b) after pore-opening etch. L_{line} is the length of the line at the tip of the inverted pyramid.

Table 2. The comparison between predicted size from ETM and measured size (100 mM KCl).

Nanopore	$G_m \pm \delta$ ($\times 10^{-8}$ S)[a]	L_{line} (nm)[b]	h (μm)	$a_p \times b_p$ (nm)[c]	$diff_m$ (nm)[d]	$a_m \times b_m$ (nm)[e]
#1	35.75 ± 0.12	312	10	561 × 249	322	600 × 278
#2	19.63 ± 0.07	222	20	340 × 118	217	375 × 158
#3	21.15 ± 0.02	221	20	354 × 133	216	385 × 169
#4	39.10 ± 0.03	553	10	755 × 202	558	758 × 200
#5	39.62 ± 0.03	463	10	695 × 232	448	724 × 276
#6	28.81 ± 0.68	51	12	329 × 278	90	412 × 322
#7	54.18 ± 0.43	394	10	802 × 408	398	798 × 400

[a] Average measured conductance and the uncertainty (δ) expressed by a standard deviation based on three continuously measured conductances.
[b] Measured length of line located in the tip of the inverted pyramid, as shown in figure 6(a).
[c] Predicted pore size from ETM using G_m. Only G_m is used because the standard deviation is too small.
[d] Calculated *diff* from $a_m - b_m$.
[e] Measured pore size from SEM image.

pyramid before the pore-opening etch, which is considered to be equal to *diff*. According to equation (2), h can be estimated from L_a. When these parameters are known, the size of pore tip (a and b) can be inferred from the measured conductance based on equation (12).

The conductance is measured in 100 mM KCl solution. Table 2 shows the comparisons between the predicted size and measured size of 7 different pyramidal silicon nanopores, including 5 samples (nanopore #1–5) in figure 4(a). It can be found that the size of most nanopores can be predicted accurately. The deviations between predicted values and measured values of these pyramidal silicon nanopores can be attributed to three reasons: (1) imperfect geometry of tip deviating from the ideal rectangle; (2) the difference between *diff* and L_{line}; (3) the error between experiments and ETM introduced in section 4.1.

Besides our work, the ability of size estimation of ETM is also evaluated by other samples from references. Because SEM images of these pyramidal silicon nanopores before pore-opening etch are unknown, *diff* is directly equal to the difference between a and b. *diff*, h and G_t of the first example [20] are 23 nm, 21 μm (estimated from the size of the front window) and 167 nS (1 M KCl), respectively. The estimated value is 12 nm × 35 nm and the measured value is 15 nm × 38 nm. The parameters of the second sample [8] are shown in figure 5. The conductance is about 50 nS (1 M KCl) estimated from the conductance-conductivity plot. Based on this value, the predicted size is 6.2 nm × 6.2 nm, which is close to the actual value—7.5 nm × 7.5 nm. Hence, it is concluded that ETM can be applied in the size estimation of the pyramidal silicon nanopore.

5. Conclusion

In summary, we proposed a new model—ETM—to describe the relationship between the conductance and the geometry of the pyramidal silicon nanopore. Different from other types of nanopores, a large half cone angle (35.3°) leads to additional resistance on ion movement, which is appeared as the decrease of diffusion coefficient. As the result, the conductivity will be smaller. After considering the effect, effective conductivity instead of intrinsic conductivity is used in the calculation of bulk conductance. Besides, equipotential rectangular disks are used for calculating access conductance due to the rectangular entrances. Compared with the

experimental results, the error of conductance predicted by ETM is less than 15%, which is better than the classical model ($\geqslant$ 25% in most cases). ETM is applicable when Du_{tip} is smaller than 0.2. At last, it is proved that ETM can predict the size of the pyramidal silicon nanopore. In addition to providing a new model, this work also points out that the decreasing diffusion coefficient needs to be noticed in other types of non-columnar channels.

Acknowledgments

This project was partially supported by National Science Foundation under Grant No. 2045169 and National Natural Science Foundation of China (Grant Nos. 62104248, 51727901, 61888102) as well as Beijing Natural Science Foundation (Grant No. 4214083).

Data availability statement

The data that support the findings of this study are available upon reasonable request from the authors.

Conflict of interest statement

The authors declare no competing financial interest.

ORCID iDs

Feibin Xiang https://orcid.org/0000-0002-9973-7074
Wenchang Zhang https://orcid.org/0000-0002-1647-7730
Shengfa Liang https://orcid.org/0000-0002-3084-8083
Weihua Guan https://orcid.org/0000-0002-8435-9672

References

[1] Ali M *et al* 2016 Label-free pyrophosphate recognition with functionalized asymmetric nanopores *Small* **12** 2014–21
[2] Li Y *et al* 2021 Engineering a smart nanofluidic sensor for high-performance peroxynitrite sensing through a spirocyclic ring open/close reaction strategy *ACS Sens.* **6** 808–14
[3] Fraccari R L *et al* 2016 High-bandwidth detection of short DNA in nanopipettes *Faraday Discuss.* **193** 459–70
[4] Weckman N E *et al* 2019 Multiplexed DNA identification using site specific dCas9 barcodes and nanopore sensing *ACS Sens.* **4** 2065–72
[5] Nouri R *et al* 2020 Sequence-specific recognition of HIV-1 DNA with solid-state CRISPR-Cas12a-assisted nanopores (SCAN) *ACS Sens.* **5** 1273–80
[6] Bell N A W and Keyser U F 2016 Digitally encoded DNA nanostructures for multiplexed, single-molecule protein sensing with nanopores *Nat. Nanotechnol.* **11** 645–51
[7] Chae H *et al* 2018 Solid-state nanopore analysis on conformation change of p53TAD–MDM2 fusion protein induced by protein–protein interaction *Nanoscale* **10** 17227–35
[8] Zeng S *et al* 2019 Rectification of protein translocation in truncated pyramidal nanopores *Nat. Nanotechnol.* **14** 1056–62
[9] Tang H *et al* 2020 Nanopore-based strategy for selective detection of single carcinoembryonic antigen (CEA) molecules *Anal. Chem.* **92** 3042–9
[10] Arjmandi N *et al* 2012 Measuring the electric charge and zeta potential of nanometer-sized objects using pyramidal-shaped nanopores *Anal. Chem.* **84** 8490–6
[11] Arjmandi N, Van Roy W and Lagae L 2014 Measuring mass of nanoparticles and viruses in liquids with nanometer-scale pores *Anal. Chem.* **86** 4637–41
[12] Wu H *et al* 2016 Translocation of rigid rod-shaped virus through various solid-state nanopores *Anal. Chem.* **88** 2502–10
[13] Cai S *et al* 2019 Small molecule electro-optical binding assay using nanopores *Nat. Commun.* **10** 1797
[14] Kaya D *et al* 2016 Effect of pore geometry on resistive-pulse sensing of DNA Using track-etched PET nanopore membrane *Electrochim. Acta* **202** 157–65
[15] Wu Y *et al* 2018 Smart DNA hydrogel integrated nanochannels with high ion flux and adjustable selective ionic transport *Angew. Chem., Int. Ed.* **57** 7790–4
[16] Kwok H, Briggs K and Tabard-Cossa V 2014 Nanopore fabrication by controlled dielectric breakdown *PLoS One* **9** e92880
[17] Roshan K A, Tang Z and Guan W 2019 High fidelity moving Z-score based controlled breakdown fabrication of solid-state nanopore *Nanotechnology* **30** 095502
[18] Chang H *et al* 2004 DNA-mediated fluctuations in ionic current through silicon oxide nanopore channels *Nano Lett.* **4** 1551–6
[19] Storm A J *et al* 2005 Translocation of double-strand DNA through a silicon oxide nanopore *Phys. Rev.* E **71** 051903
[20] Park S R, Peng H and Ling X S 2007 Fabrication of nanopores in silicon chips using feedback chemical etching *Small* **3** 116–9
[21] Albrecht T, Gibb T and Nuttall P 2013 Ion transport in nanopores *Engineered Nanopores for Bioanalytical Applications* (Oxford: William Andrew Publishing) pp 1–30 ch 1
[22] Lee C *et al* 2012 Large apparent electric size of solid-state nanopores due to spatially extended surface conduction *Nano Lett.* **12** 4037–44
[23] Smeets R M M *et al* 2008 Noise in solid-state nanopores *Proc. Natl. Acad. Sci.* **105** 417
[24] Smeets R M M, Dekker N H and Dekker C 2009 Low-frequency noise in solid-state nanopores *Nanotechnology* **20** 095501
[25] Kong J *et al* 2019 Specific biosensing using DNA aptamers and nanopores *Adv. Funct. Mater.* **29** 1807555
[26] Yusko E C *et al* 2017 Real-time shape approximation and fingerprinting of single proteins using a nanopore *Nat. Nanotechnol.* **12** 360–7
[27] Liebes Y *et al* 2010 Reconstructing solid state nanopore shape from electrical measurements *Appl. Phys. Lett.* **97** 223105
[28] Kowalczyk S W *et al* 2011 Modeling the conductance and DNA blockade of solid-state nanopores *Nanotechnology* **22** 315101
[29] Nouri R, Tang Z and Guan W 2019 Calibration-free nanopore digital counting of single molecules *Anal. Chem.* **91** 11178–84
[30] Zwanzig R 1992 Diffusion past an entropy barrier *J. Phys. Chem.* **96** 3926–30
[31] Wen C, Zhang Z and Zhang S-L 2017 Physical model for rapid and accurate determination of nanopore size via conductance measurement *ACS Sens.* **2** 1523–30
[32] Wen C *et al* 2019 On rectification of ionic current in nanopores *Anal. Chem.* **91** 14597–604

[33] Frament C M and Dwyer J R 2012 Conductance-based determination of solid-state nanopore size and shape: an exploration of performance limits *J. Phys. Chem.* C **116** 23315–21
[34] Hille B 1968 Pharmacological modifications of the sodium channels of frog nerve *J. Gen. Physiol.* **51** 199–219
[35] Lossel Y Y, Kochanov E S and Strunskii M G 1971 Capacitance of flat plates *The Calculation of Electrical Capacitance* (Ohio: Foreign Technology Division) pp 121–3 ch 4
[36] Smeets R M M *et al* 2006 Salt dependence of ion transport and DNA translocation through solid-state nanopores *Nano Lett.* **6** 89–95
[37] Burada P S *et al* 2007 Biased diffusion in confined media: test of the fick-jacobs approximation and validity criteria *Phys. Rev.* E **75** 051111
[38] Chávez Y, Chacón-Acosta G and Dagdug L 2018 Effects of curved midline and varying width on the description of the effective diffusivity of brownian particles *J. Phys. Condens. Matter* **30** 194001
[39] Kovarik M L, Zhou K and Jacobson S C 2009 Effect of conical nanopore diameter on ion current rectification *J. Phys. Chem.* B **113** 15960–6
[40] Apel P Y *et al* 2011 Effect of nanopore geometry on ion current rectification *Nanotechnology* **22** 175302
[41] Hall J E 1975 Access resistance of a small circular pore *J. Gen. Physiol.* **66** 531–2
[42] Kalinay P and Percus J K 2005 Projection of two-dimensional diffusion in a narrow channel onto the longitudinal dimension *J. Chem. Phys.* **122** 204701
[43] Berezhkovskii A and Szabo A 2011 Time scale separation leads to position-dependent diffusion along a slow coordinate *J. Chem. Phys.* **135** 074108
[44] Dagdug L and Pineda I 2012 Projection of two-dimensional diffusion in a curved midline and narrow vvarying width channel onto the longitudinal dimension *J. Chem. Phys.* **137** 024107
[45] McKee C B 2009 An accurate equation for the electrolytic conductivity of potassium chloride solutions *J. Solut. Chem.* **38** 1155–72
[46] Poggioli A R, Siria A and Bocquet L 2019 Beyond the tradeoff: dynamic selectivity in ionic transport and current rectification *J. Phys. Chem.* B **123** 1171–85
[47] Dal Cengio S and Pagonabarraga I 2019 Confinement-controlled rectification in a geometric nanofluidic diode *J. Chem. Phys.* **151** 044707
[48] Kontturi K, Murtomäki L and Manzanares J A 2008 Transport in membranes *Ionic Transport Processes: in Electrochemistry and Membrane Science* (Oxford: Oxford University Press) pp 152–7
[49] Kox R *et al* 2009 Shrinking solid-state nanopores using electron-beam-induced deposition *Nanotechnology* **20** 115302
[50] Chen Q *et al* 2017 SEM-induced shrinkage and site-selective modification of single-crystal silicon nanopores *Nanotechnology* **28** 305301
[51] Yuan Z, Lei X and Wang C 2020 Controllable fabrication of solid state nanopores array by electron beam shrinking *Int. J. Mach. Tools Manuf.* **159** 103623